Quantitative determination of the Mn site distribution in ultrathin $Ga_{0.80}Mn_{0.20}As$ layers with high critical temperatures: A Rutherford backscattering channeling investigation

D. Benzeggouta,[1] Kh. Khazen,[2] I. Vickridge,[1,3] H. J. von Bardeleben,[1,3] L. Chen,[4] X. Z. Yu,[4] and J. H. Zhao[4]

[1]*Sorbonne Universités, UPMC Université Paris 06, UMR7588, Institut des NanoSciences de Paris, F-75005, Paris, France*

[2]*Sorbonne Universités, UPMC Université Paris 06, Laboratoire des Matériaux Mésoscopiques et Nanométriques, F-75005, Paris, France*

[3]*CNRS, UMR7588, Institut des NanoSciences de Paris, F-75005, Paris, France*

[4]*State Key Laboratory of Superlattices and Microstructures, Institute of Semiconductors, Chinese Academy of Sciences, P. O. Box 912, Beijing 100083, China*

(Received 14 November 2013; revised manuscript received 18 March 2014; published 31 March 2014)

The Mn dopant distribution in ultrathin (20 nm) highly doped (nominal $x = 0.20$) $Ga_{1-x}Mn_xAs$ epitaxial films with critical temperatures close to 175 K and magnetization of 100 emu/cm^3 is analyzed by Rutherford backscattering spectrometry (RBS) in a random and channeling configuration. We could quantify the total concentration and the respective fraction of substitutional, interstitial, and random site Mn ions in as-grown and annealed samples. The measured total Mn concentration is $x = 0.23$. In the as-grown state 30% of the Mn dopant is located on interstitial sites. Thermal annealings at 180 °C for several hours monotonically reduce the interstitial Mn fraction to 11%. Simultaneously the fraction of randomly located Mn is increased by the same amount. The substitutional Mn concentration is stable under these annealing conditions. The effective Mn concentration could be increased to $x = 0.13$. However, the critical temperature does not increase proportionally with the magnetization. A comparison of the magnetization values demonstrates that the interstitial Mn ions are already incorporated during the growth in the form of Mn_{Ga}-Mn_i clusters.

DOI: 10.1103/PhysRevB.89.115323 PACS number(s): 75.50.Pp, 29.30.−h, 75.30.−m

I. INTRODUCTION

The dilute ferromagnetic semiconductor (DMS) $Ga_xMn_{1-x}As$ has been widely studied in the last decade for its model character as a spintronics material [1–3]. For GaMnAs to be useful in device applications, it would be necessary to increase its Curie temperature T_C above room temperature. The highest temperature so far achieved is close to 200 K and requires the use of ultrathin layers [4]. In principle, room temperature ferromagnetism is predicted in the mean-field model to occur for an uncompensated Mn_{Ga} doping level x of 0.125 and a hole carrier concentration of 3.5×10^{20} cm^{-3} [2]. To understand the limitations of obtaining higher critical temperatures, a quantitative knowledge of the principal parameters such the Mn dopant concentration and its distribution in the lattice is required. As standard techniques such as secondary ion mass spectroscopy (SIMS) are not sufficiently quantitative to measure directly the Mn concentration in such thin layers, its value is often just extrapolated from measurements of very thick films grown under similar conditions. But this information is biased due to an inhomogeneous Mn distribution in layers above typically 50 nm thickness. In addition, the information on the site distribution is of course not accessible with SIMS measurements. Whereas the same limitation applies to RBS measurements in random configuration, it can be overcome by RBS channeling measurements where the backscattering yield depends strongly on the lattice position of the scattering centers.

Different limiting factors for increasing the T_C have been identified but the discussion is still controversial [5–8]. Whereas generally highest uncompensated hole concentrations are believed to lead to highest T_C, more recently partially compensated samples have been proposed to be optimal [6,7]. The effective Mn doping concentration (x_{eff}), defined as the fraction of noncompensated substitutional Mn ions, is equally a related key element in this discussion, but direct measurements of the total Mn content and the distribution of Mn over the substitutional and interstitial lattice sites in ultrathin layers had not yet been reported; most models were just based on estimated effective Mn concentrations [8–17]. Until recently, the effective Mn concentrations seemed to be limited to $x_{\text{eff}} \leqslant 0.05$ even though much higher ($x = 0.20$) total Mn concentration have been attained. The reason is well known: For high doping levels Mn is not only incorporated on Ga lattice sites but also occupies more and more interstitial sites and may even form MnAs precipitates. Among the different configurations, only isolated Mn ions on Ga lattice sites (Mn_{Ga}) are ferromagnetically active. Mn on interstitial sites (Mn_i) will act in two ways: it can compensate the magnetic moments of Mn_{Ga}, through formation of antiferromagnetically coupled Mn_{Ga}-Mn_i pairs, which reduces Mn_{eff}, the number of magnetically effective Mn_{Ga} ions, and second, the isolated Mn_i ion is a double donor reducing the free hole concentration and thus equally T_C. However, the fraction of isolated and paired Mn_i could not be determined directly. A quantitative study of the Mn distribution in highly doped samples is thus of interest if one wants to model the magnetic properties of these layers.

It is useful to recall that the global composition $Ga_{1-x}Mn_xAs$ represents a large family of materials with quite different properties depending on the total doping concentration, the Mn distribution over the different lattice sites, and the layer thickness. Thus results obtained for low-doped thick layers (such as 100 nm) are not necessarily valid for highly doped ultrathin layers. We can schematically classify these materials into three groups: marginally ferromagnetic ($x \leqslant 0.02$) with impurity band conduction, weakly compensated ferromagnetic ($x = 0.05$), and heavily doped,

highly compensated ferromagnetic layers ($x > 0.10$) with metallic conduction. Above 50 nm thickness the layers are increasingly inhomogeneous in the Mn depth distribution, and the post growth thermal annealing applied to optimize the magnetic properties increases this inhomogeneity even further. Clearly a layer thickness of $\leqslant$20 nm layers seems most suited for obtaining homogeneous thin films with highest T_C values.

In the as-grown state epitaxial GaMnAs films are not yet magnetically optimized as far as the saturation magnetization, the free hole concentration, and T_C are concerned and post growth thermal annealing in the 150 to 200 °C range have shown to be efficient to improve these properties substantially. It is generally assumed that the mechanism responsible is the outdiffusion of Mn_i to the surface, whereas the substitutional Mn_{Ga} ions, which have a higher thermal stability, are not displaced. However, quantitative measurements of the Mn distribution in thin (<20 nm) layers have not yet been published. Previously, high resolution x-ray diffraction (HRXRD), transmission electron microscopy (HRTEM), and channeling particle induced x-ray emission (c-PIXE) studies of thick (> 100 nm) samples have been undertaken, in order to measure or more precisely, estimate the substitutional and interstitial Mn concentrations in highly doped annealed films [8–17]. The difficulties for deducing Mn_{Ga} and Mn_i densities from x-ray diffraction measurements have been discussed in [15], where in spite of using 100 nm thick layers the absolute amounts of Mn_{Ga} and Mn_i could not be determined. A later HRXRD and x-ray absorption study revealed an additional difficulty often encountered in layers with thickness above 50 nm: a vertical inhomogeneity in the Mn distribution which is further amplified by the post growth annealing procedure. In Ref. [16] the inhomogeneous distribution was treated in a simplified two-layer box model. Previous c-PIXE measurements on 100 nm thick samples suffered from flux peaking effects, which were not quantified and thus allowed only a "rough estimation" of the Mn_i concentration [8].

In this work we present the results of an RBS channeling analysis of the Mn site distribution in 20 nm highly doped ($x_{nominal} = 0.20$) $Ga_{1-x}Mn_xAs$ films with close to record magnetic properties of $M_{sat} = 100$ emu/cm^3 and critical temperatures of 175 K. In particular we have analyzed these films in the as-grown and thermally annealed state to relate the modified magnetic properties with the Mn redistributions.

II. EXPERIMENTAL METHODS

$Ga_{1-x}Mn_xAs$ films of 20 nm thickness with a nominal Mn content of $x = 0.20$ were grown by low-temperature molecular-beam epitaxy. First, an epitaxial 200 nm GaAs undoped buffer layer was grown on (001) oriented semi-insulating GaAs substrates, then the 20 nm thin Mn doped film was grown without growth interruption on the rotating substrate. Typical conditions are a growth temperature of 250 °C and a beam equivalent pressure (BEP) ratio Mn/Ga of 0.14. To avoid thermal oxidation of the GaMnAs films when exposed to ambient conditions, they were capped by a 0.5 nm GaAs layer. Thermal annealing was carried out in air at 180 °C for different periods. Three samples are investigated here: as-grown (AG); annealed for 6 h at 180 °C (ANN1); and annealed for 10 h at 180 °C (ANN2). More details on the sample growth and annealing effects have been published recently [18].

The homogeneity of the samples was verified by X-band ferromagnetic resonance spectroscopy. The three types of layers were characterized by a single uniform mode spectrum with an exceptionally small linewidth of 50 Oe.

The Rutherford backscattering spectrometry measurements were performed with the Van de Graaff accelerator of the SAFIR platform of the Université Pierre et Marie Curie. We used a 1.8 MeV $^4He^+$ beam of 1 mm diameter. As the beam penetrates several 100 nm into the sample, the GaMnAs film is analyzed over its entire thickness, with depth resolution determined by the energy resolution of the detector. Scattered particles were detected with a semiconductor detector placed at 165°, with the detector solid angle determined by use of a Bi-implanted silicon reference sample. Dead time and pileup were kept to low levels.

Flux peaking effects can be neglected for such ultrathin layers. In ion channeling, the flux of incident particles, initially uniform at the surface of the crystal, is substantially modified as the particles suffer a series of correlated elastic interactions, mediated by the screened Coulomb potential, with the rows of atomic nuclei of the crystals. At sufficient depth (>100 nm) the flux distribution attains a statistical equilibrium [19] in which the flux is concentrated in the center of the channels, far from the atomic rows. For the thin samples (20 nm) investigated here, the flux is still far from the equilibrium distribution and the flux at the center of the channels (where the Mn_i is visible) is practically unchanged from the average flux. An example of flux distributions at 20 and 100 nm for ^4He in a UO_2 crystal may be found in [20] where it is clear that the flux in the central region of the channels, at 20 nm depth, is essentially still just the mean flux. We have assumed therefore that for these thin GaMnAs films, flux peaking may be ignored. The GaMnAs samples were aligned with respect to the beam with a six-axis goniometer for channeling measurements. Channeled spectra were summed for successive 1 μC doses to avoid irradiation-induced damage. The random spectra were obtained by averaging the spectra from a 90° azimuthal scan with the sample tilted a few degrees away from the axial channeling direction.

The magnetization measurements $M(H)$ and $M(T)$ were performed with a commercial SQUID magnetometer.

III. RESULTS AND DISCUSSION

In Fig. 1 we show a typical $M(T)$ curve for the as-grown and annealed samples. From hysteresis measurements $M(H)$ we determine the saturation magnetization at $T = 4.5$ K to be $M^{AG} = 71$ emu/cm^3, $M^{ANN1} = 80$ emu/cm^3, and $M^{ANN2} = 103$ emu/cm^3. The high magnetization value for the as-grown sample is already remarkable. Typical maximum values published previously, even after thermal annealing, are only in the 50 emu/cm^3 range. The $M(T)$ curve (Fig. 1) was measured by plotting the remnant magnetization at each temperature. We obtain critical temperatures of $T_C{}^{AG} = 145$ K, $T_C{}^{ANN1} = 175$ K, and $T_C{}^{ANN2} = 165$ K.

In the RBS analysis we will distinguish three types of Mn atoms: Mn on Ga substitutional sites (Mn_{Ga}), Mn on

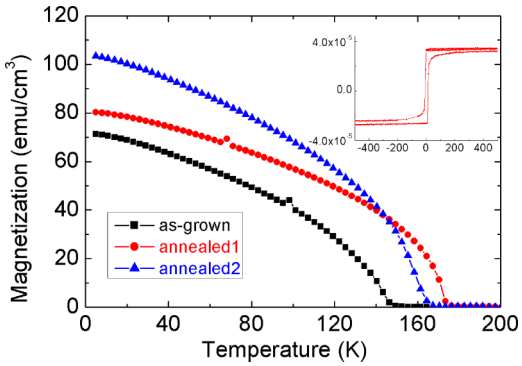

FIG. 1. (Color online) Saturation magnetization as a function of temperature for as-grown, annealed 1, and annealed 2 20 nm thick $Ga_{0.80}Mn_{0.20}As$ samples. The inset shows the magnetization M (emu) as a function of the magnetic field H (Oe) at 4.5 K for sample annealed 1.

tetrahedral interstitial sites (Mn_i), and Mn at random locations incommensurate with the zinc-blende lattice (Mn_R). Thus the total projected areal density $\{Mn_{tot}\}$ is given by the sum of $\{Mn_{Ga}\} + \{Mn_i\} + \{Mn_R\}$. Mn_R is observable for all directions of the channeling beam. Mn_i is observable for channeling along the ⟨110⟩, axis but shadowed along the ⟨001⟩ axis, and Mn_{Ga} is shadowed for all channeling directions. By comparing the yield of incident ions scattered from Mn with the beam in a random direction or aligned along ⟨001⟩ Mn_{001}, and along ⟨110⟩ Mn_{110}, we can determine the different fractions of $\{Mn_{Tot}\}$, $\{Mn_R\}$, and $\{Mn_i\} + \{Mn_R\}$, respectively, from which we deduce $\{Mn_{Ga}\}$.

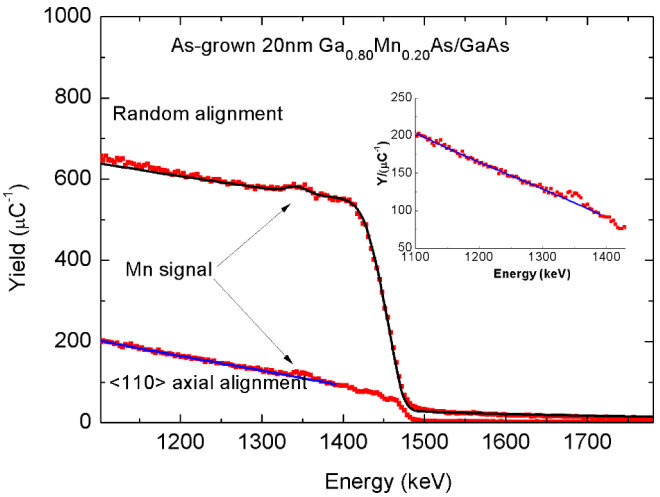

FIG. 2. (Color online) Random and ⟨110⟩ axially channeled RBS spectra from a 20 nm as-grown $Ga_{0.80}Mn_{0.20}As$ film on GaAs. The formula indicates the nominal Mn concentration, the actual one, slightly higher, is given in Table I. The black line is a simulation made with SimNRA [21], including the effects of pileup and deadtime. The blue line on the channeled spectrum shows a typical third-order polynomial fit to the channeled spectrum in the vicinity of the peak from Mn in the GaMnAs layer, used to estimate the background under the Mn peak in order to determine the peak area. The inset shows a zoom of the ⟨110⟩ channeled spectrum.

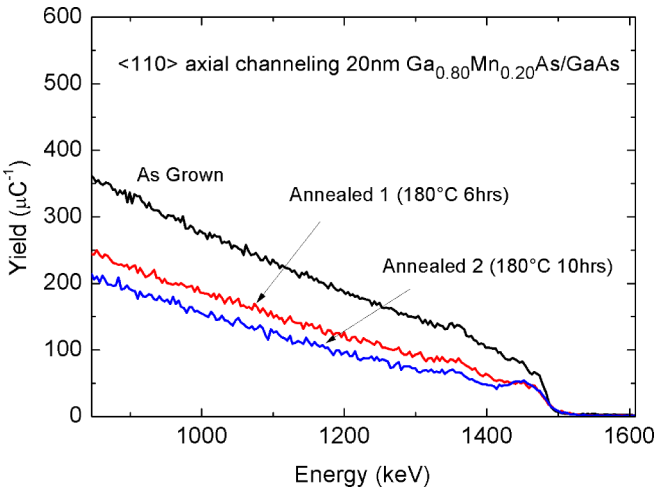

FIG. 3. (Color online) ⟨110⟩ axial RBS-channeling spectra of 20 nm GaMnAs before and after annealing. The as-grown minimum yield is 7%, which indicates that the buffer layer is of lower crystalline quality than the GaAs substrate, which has a minimum yield of 2%–3%. The minimum yield reduces monotonically with anneal duration, indicating improving crystalline quality of the buffer layer as annealing proceeds.

Figure 2 shows a random RBS spectrum from the as-grown sample. The Mn signal is superposed on the intense plateau from the Ga and As of the substrate. Figure 2 shows typical random and ⟨110⟩ channeled spectra for the as-grown sample. The fit to the random spectrum was performed with the SimNra program [21]. This program neglects the crystal structure and uses only the composition of the material to calculate the backscattering spectrum. For the channeled spectra (Figs. 2 and 3) we found that subtracting a third-order polynomial was adequate to extract the Mn signal, allowing reliable estimation of peak areas. Although the uncertainty in the determination of the peak areas is determined by both the counting statistics and the uncertainty in the polynomial fit, it is dominated by the counting statistics.

The minimum channeling yield X_{min} is about 7%. It should be noted that this minimum yield is dominated by the contribution of the underlying buffer layer; its high value indicates that the low temperature buffer layer is of lower crystalline quality than the high quality GaAs substrate, for which X_{min} of 2%–3% is obtained; it is not possible from these spectra to determine the X_{min} for the GaMnAs layer.

Table I summarizes the respective values of $\{Mn\}$ obtained from the RBS-c measurements, and Fig. 4 shows the evolution of these values as a function of annealing time. We first note that the total Mn concentration$\{Mn_{tot}\}$ measured by RBS is slightly superior to the nominal value targeted by the growth conditions. In fact an areal density of 10.4×10^{15} cm^{-2} corresponds to an x value of $x = 0.24$. This result highlights the recurrent difficulty of how to measure directly the dopant concentration in such a thin layer. The fraction of interstitial Mn in the as-grown state is very high, nearly 30%. Such a value is not unexpected for this doping level. Indeed, whereas for low dopant concentrations ($x \leq 0.02$) all Mn ions are incorporated substitutionally, above $x = 0.05$ the fraction of Mn ions on interstitial sites increases dramatically [22]. The

TABLE I. $\{Mn_{tot}\}$, $\{Mn_R\}$, $\{Mn_i\}$, $\{Mn_{Ga}\}$, and $\{Mn_{eff}\}$ concentrations obtained from RBS-c measurements. Upper values are in units of 10^{15} at/cm^2, lower values are x in percent. For the channeling spectra, the theoretical contribution of the channeling surface peak to the Mn peak areas was subtracted. Values in parentheses (*in italics*) are the 1σ uncertainties due to the counting statistics of the RBS spectra. M is the magnetization value predicted from the RBS results assuming $\{Mn_{eff}\} = \{Mn_{Ga}\} - \{Mn_i\}$and M_{sat} is the one measured by SQUID. In the last row we give the critical temperatures T_C.

		$\{Mn_{tot}\}$	$\{Mn_R\}+\{Mn_i\}\langle 110\rangle$	$\{Mn_R\}\langle 100\rangle$	$\{Mn_i\}$	$\{Mn_{Ga}\}$	$\{Mn_{eff}\}$	M (emu/cm^3) RBS	M_{sat} (emu/cm^3) SQUID	T_C (K)
As-grown	C /10^{15} cm^{-2}	10.4(*0.5*)	3.9(*0.7*)	0.8(*0.16*)	3.1(*0.86*)	6.5(*1.2*)	3.4	68	71	145
	x (%)	*23*	*8.7*	*1.8*	*7.0*	*14.6*	*7.6*			
Anneal 1	C /10^{15} cm^{-2}	10.7(*0.5*)	3.9(*0.5*)	2.2(*0.26*)	1.7(*0.76*)	6.8(*1*)	5.1	102	80	175
	x (%)	*24*	*8.7*	*4.9*	*3.8*	*15.2*	*11.4*			
Anneal 2	C /10^{15} cm^{-2}	10.7(*0.5*)	3.7(*0.7*)	2.5(*0.23*)	1.2(*0.93*)	7.0(*1.2*)	5.8	116	103	165
	x (%)	*24*	*8.7*	*5.6*	*2.7*	*15.7*	*13*			

comparison of the RBS results obtained in random and $\langle 110\rangle$ configuration show that the annealing process used in this work leaves $\{Mn_{tot}\}$ and $\{Mn_R + Mn_i\}$ practically unchanged. Thus the $\{Mn_{Ga}\}$ concentration is not modified by the annealing. The main effect of the annealing is the respective redistribution between Mn_R and Mn_i ions. As expected, $\{Mn_i\}$ decreases with the annealing, and $\{Mn_R\}$ increases—in accordance with the view that the Mn_i ions diffuse to the surface where they are oxidized or form MnAs precipitates during annealing; these Mn atoms are seen as Mn_R. Contrary to what might have been expected, there is still a significant interstitial fraction left ($x = 0.027$) after the second anneal. We observe that the T_C decreases for the longer annealing time even though M_{sat} still increases. This is *a priori* surprising. Possible explanations are a decrease in the hole concentration (not measured here), a decrease in the mean-free path of the holes [23], or a band filling effect.

The distribution of interstitial Mn ions in as-grown and annealed layers is an important issue: Will they form close pairs with the substitutional Mn ions or will they remain isolated on tetrahedral sites? Most authors assume ad hoc a 100% pair formation in the as-grown state and complete out-diffusion by annealing, but quantitative experimental results were not available. We show here that in fact the magnetization values can be used to solve this issue. The magnetization at saturation is mainly given by $g_{Mn}S_{Mn}\mu_B Mn_{eff}$, where $g_{Mn} = 2$ is the Landé factor for the Mn^{2+} ions and $S_{Mn} = 5/2$ is the spin of the Mn ion. Typical experimental values of the average magnetic moment per Mn ion taking into account the antiferromagnetic contribution of the (weakly polarized) holes are 4.3 μ_B [24]. We will now consider two extreme cases: either the interstitial Mn ions are not associated with Mn_{Ga}, in which case $\{Mn_{eff}\} = \{M_{Ga}\}$ or they are fully associated and thus $\{Mn_{eff}\} = \{Mn_{Ga}\} - \{Mn_i\}$. The comparison of the magnetization values (Table I) measured by SQUID with those calculated from the RBS results shows that only the second model is compatible with the experimental results. The agreement between the magnetization deduced from the c-RBS measurements and that measured by SQUID is rather satisfactory for the AG and ANN2 samples. For the ANN1 sample, which has the highest Curie temperature, the agreement is less good. For both annealed samples the predicted magnetization value is higher than the measured one. This observation might indicate a reduction of the thickness of the magnetically active part of the layer by the annealing process which has not been considered here.

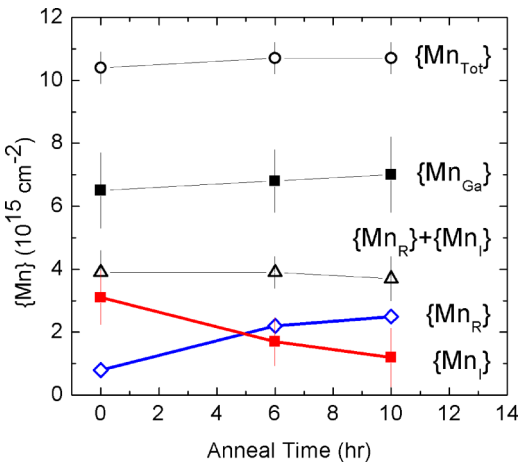

FIG. 4. (Color online) Amounts of Mn in various sites (see text) as a function of annealing time. The evolution of $\{Mn_i\}$ and $\{Mn_R\}$ is highlighted by the red and blue lines joining the symbols. The estimated uncertainties ($\pm 1\sigma$) in $\{Mn\}$ are indicated by the vertical lines on each symbol.

IV. CONCLUSIONS

Channeling RBS has been shown to be able to analyze quantitatively the Mn distribution in 20 nm thin highly doped GaMnAs films. The total Mn concentration of $x = 0.24$ is close to the targeted nominal value of $x = 0.20$. The fraction of interstitial Mn ions is nearly 30% of the total Mn concentration in the as-grown state. Its fraction is reduced by a factor of 3 by the annealing but remains significant after the second annealing. The substitutional Mn fraction is not modified under these conditions. The annealed sample has an effective Mn concentration of $x = 0.11$, but its T_C is still below 200 K. Our results indicate that still higher critical

temperatures should be obtainable by further optimizing the layer thickness, the total initial Mn concentration, and the annealing procedures to further diminish the Mn_i fraction.

ACKNOWLEDGMENTS

This work has been partially supported by an ANR grant "2010-Blanc-0424-02" and performed within the framework of the SAFIR Platform of UPMC.

[1] H. Ohno, A. Shen, F. Matsukura, A. Oiwa, A. Endo, S. Katsumoto, and Y. Iye, Appl. Phys. Lett. **69**, 363 (1996).
[2] T. Dietl, H. Ohno, and F. Matsukura, Phys. Rev. B **63**, 195205 (2001).
[3] T. Jungwirth, J. Sinova, J. Masek, J. Kucera, and A. H. MacDonald, Rev. Mod. Phys. **78**, 809 (2006).
[4] L. Chen, X. Yang, F. Yang, J. Zhao, J. Misuraca, P. Xiong, and S. von Molnár, Nano Lett. **11**, 2584 (2011).
[5] T. Jungwirth, K. Y. Wang, J. Mašek, K. W. Edmonds, J. König, J. Sinova, M. Polini, N. A. Goncharuk, A. H. MacDonald, M. Sawicki, A. W. Rushforth, R. P. Campion, L. X. Zhao, C. T. Foxon, and B. L. Gallagher, Phys. Rev. B **72**, 165204 (2005).
[6] M. Dobrowolska, K. Tivakornsasithorn, X. Liu, J. K. Furdyna, M. Berciu, K. M. Yu, and W. Walukiewicz, Nat. Mater. **11**, 444 (2012).
[7] N. Samarth, Nat. Mater. **11**, 360 (2012).
[8] K. M. Yu, W. Walukiewicz, T. Wojtowicz, I. Kuryliszyn, X. Liu, Y. Sasaki, and J. K. Furdyna, Phys. Rev. B **65**, 201303 (2002).
[9] M. Wang, K. W. Edmonds, B. L. Gallagher, A. W. Rushforth, O. Makarovsky, A. Patane, R. P. Campion, C. T. Foxon, V. Novak, and T. Jungwirth, Phys. Rev. B **87**, 121301 (2013).
[10] K. M. Yu, W. Walukiewicz, T. Wojtowicz, W. L. Lim, X. Liu, U. Bindley, M. Dobrowolska, and J. K. Furdyna, Phys. Rev. B **68**, 041308 (2003).
[11] K. W. Edmonds, P. Bogusławski, K. Y. Wang, R. P. Campion, S. N. Novikov, N. R. S. Farley, B. L. Gallagher, C. T. Foxon, M. Sawicki, T. Dietl, M. Buongiorno Nardelli, and J. Bernholc, Phys. Rev. Lett. **92**, 037201 (2004).
[12] K. Y. Wang, K. W. Edmonds, R. P. Campion, B. L. Gallagher, N. R. S. Farley, C. T. Foxon, M. Sawicki, P. Boguslawski, and T. Dietl, J. Appl. Phys. **95**, 6512 (2004).
[13] K. M. Yu, W. Walukiewicz, T. Wojtowicz, W. L. Lim, X. Liu, M. Dobrowolska, and J. K. Furdyna, Nucl. Instrum. Methods Phys. Res. Sect. B **219–220**, 636 (2004).
[14] F. Glas, G. Patriarche, L. Largeau, and A. Lemaître, Phys. Rev. Lett. **93**, 086107 (2004).
[15] V. Holy, Z. Matej, O. Pacherova, V. Novak, M. Cukr, K. Olejnik, and T. Jungwirth, Phys. Rev. B **74**, 245205 (2006).
[16] L. Horak, J. Matejova, X. Marti, V. Holy, V. Novak, Z. Soban, S. Mangold, and F. Jimenez-Villacorta, Phys. Rev. B **83**, 245209 (2011).
[17] K. M. Yu, W. Walukiewicz, T. Wojtowcz, J. Denlinger, M. A. Scarpulla, X. liu, and J. K. Furdyna, Appl. Phys. Lett. **86**, 042102 (2005).
[18] H. L. Wang, L. Chen, and J. Zhao, Sci. China Phys. Mech. Astron. **56**, 99 (2013).
[19] L. C. Feldman, J. W. Mayer, S. T. Picraux, *Materials Analysis by Ion Channeling* (Academic, New York, 1983).
[20] L. Nowicki, A. Turos, R. Ratajczak, A. Stonert, and F. Garrido, Nucl. Instrum. Methods Phys. Res. Sect. B **240**, 277 (2005).
[21] M. Mayer, http://home.rzg.mpg.de/~mam/References.html, 1999.
[22] Kh. Khazen, Ph.D. thesis, Université Pierre et Marie Curie, Paris, 2008.
[23] Kh. Khazen, H. J. von Bardeleben, J. L. Cantin, A. Mauger, L. Chen, and J. H. Zhao, Phys. Rev. B **81**, 235201 (2010).
[24] T. Jungwirth, J. Mašek, K. Y. Wang, K. W. Edmonds, M. Sawicki, M. Polini, Jairo Sinova, A. H. MacDonald, R. P. Campion, L. X. Zhao, N. R. S. Farley, T. K. Johal, G. van der Laan, C. T. Foxon, and B. L. Gallagher, Phys. Rev. B **73**, 165205 (2006).